A SURVEY OF LARGE MOLECULES TOWARD THE PROTO–PLANETARY NEBULA CRL 618

Anthony J. Remijan,[1,2,3] Friedrich Wyrowski,[4] Douglas N. Friedel,[1] David S. Meier,[1] and Lewis E. Snyder[1]

ABSTRACT

We present the results of our survey toward the proto–planetary nebula CRL 618 for several large, highly saturated, oxygen-bearing organic molecules of biological importance including acetaldehyde (CH_3CHO), acetic acid (CH_3COOH), dimethyl ether (CH_3OCH_3), ethanol (CH_3CH_2OH), formic acid (HCOOH) and methyl formate ($HCOOCH_3$); large carbon chain molecules including methyl cyanide (CH_3CN), methylcyanoacetylene (CH_3C_3N), cyanoacetylene (HC_3N), cyanodiacetylene (HC_5N), and C_6H; and, finally, smaller molecules including ^{34}SO, SO_2, $OC^{34}S$, and MgNC. No biologically important organic molecules were detected. However, we report the first interferometric detections of CH_3CN and vibrationally excited HC_3N and HC_5N toward this source. The temperature and distribution of CH_3CN toward CRL 618 indicates that it is formed in the outer envelope surrounding the ultracompact H II region. Furthermore, the P Cygni line profile and corresponding channel maps of vibrationally excited HC_5N support its distribution in the extended envelope expanding radially from the central star. The detection of vibrationally excited HC_3N confirmed the temperature structure and column density of HC_3N in the inner envelope found by Wyrowski and colleagues. Finally, our observations clearly indicate that CRL 618 is a good source of large carbon chain species but a very poor source for detecting or producing organic species of biological importance.

Subject headings: line: identification — radio lines: stars — stars: AGB and post-AGB — stars: individual (CRL 618)

1. INTRODUCTION

Recently, there have been several surveys for complex molecular species toward massive star-forming regions including W75N, G45.47+0.05, G19.61−0.23 (Remijan et al. 2004a), and Sgr B2(N-LMH) (Hollis et al. 2004; Friedel et al. 2004; Snyder et al. 2002). These massive star-forming regions all have very similar physical conditions. First, they are rich in interstellar dust. Many molecular species, even H_2, appear to have their origins on the icy surfaces of dust grains (Hollenbach & Salpeter 1971). Dust becomes more important as more complex molecules are found in the interstellar medium (ISM). The abundances of large molecules in several regions are much larger than the predicted abundances from ion-molecule gas-phase chemistry models (Remijan et al. 2002; Mehringer & Snyder 1996). Thus, grain surface chemistry has been invoked to account for the large abundance of complex interstellar molecules. Second, the high density of gas and dust limit the amount of UV flux. This is important because UV photons destroy complex molecules (Ehrenfreund et al. 2001). Finally, the hot-core regions have high temperatures. It is generally believed that molecules formed via grain surface reactions in a cold-collapse phase are then evaporated by thermal heating and thereafter deposited into the gas phase. Typically, if the temperature of dust grains exceeds 100 K, the mantles evaporate, and species that were frozen on the grain can now escape into the gas phase (Tielens & Hagen 1982; Hasegawa et al. 1992). Furthermore, an interesting warm gas-phase chemistry may take place after the molecules are evaporated, leading to the production of even more complex molecules. Thus, these regions appear to be ideal environments for complex interstellar chemistry. It is logical to assume that similar regions rich in dust, with high density and near a source of high temperature, i.e., O and B stars or ultracompact (UC) H II regions, should also contain the necessary chemistry to synthesize large molecular species.

Another astronomical environment that appears to fit the above selection criteria is the extended envelope of proto–planetary nebulae (PPNe). The PPN phase of stellar evolution occurs at the end of the asymptotic giant branch (AGB) stage, in which substantial mass loss is taking place, and before the formation of the white dwarf, after which the temperature becomes high enough to ionize the extended envelope and start the formation of a planetary nebula. This phase of stellar evolution is typically very short, lasting only about 10 thousand years. However, during that time a very interesting chemistry may take place in the extended envelope of the post-AGB star. Thus, the extended envelopes of PPNe may be ideal chemical factories to produce large molecules and molecules of biological importance.

CRL 618 (AFGL 618, IRAS 04395+3601) is a carbon-rich, evolved PPN with a thick molecular envelope surrounding a B0 star and an UC H II region (Cernicharo et al. 2001b). However, the complete physical structure of CRL 618 is very complex. CRL 618 has been observed in several molecular species at different resolutions and wavelengths. Some of its distinct structures include optical high-velocity bipolar outflows (Trammell 2000), a central UC H II region, a low-velocity, expanding torus of molecular emission, and an extended, expanding AGB envelope (Sanchez Contreras & Sahai 2004). In addition to several individual structures, the circumstellar envelope (CSE) itself also shows a complex structure and is predicted to exhibit a complex distribution of several different molecular species (Woods et al. 2003). Thus, by observing the molecular envelope in several different molecular species at different excitation temperatures, we can obtain a better understanding of the temperature and density structure of the CSE. Furthermore, the interactions of the

[1] Department of Astronomy, 103 Astronomy Building, 1002 West Green Street, University of Illinois, Urbana, IL 61801; friedel@astro.uiuc.edu, meierd@astro.uiuc.edu, snyder@astro.uiuc.edu.

[2] Current address: NASA Goddard Space Flight Center, Earth and Space Data Computing Division, Code 930, Greenbelt, MD 20771; aremijan@pop900.gsfc.nasa.gov.

[3] National Research Council Resident Research Associate.

[4] Max-Planck-Institut für Radioastronomie, Auf dem Hügel 69, D-53121 Bonn, Germany; wyrowski@mpifr-bonn.mpg.de.

TABLE 1
Observational Parameters

Observation Date (1)	Gain Calibrator (2)	Flux Calibrator (3)	Frequency (GHz) (4)	Array (5)	Beam (arcsec × arcsec) (6)
2002 Oct 11	0359+509	Saturn	111.5	C	7.18 × 6.59
2002 Oct 19	0359+509	Saturn	111.5	C	6.97 × 6.50
2002 Nov 4	0359+509	Jupiter	110.3	C	6.91 × 6.43
2002 Nov 18	0359+509	Saturn	111.5	C	7.46 × 6.66
2003 Jan 28	0359+509	Jupiter	110.3	B	2.90 × 1.84
2003 Jan 31	0359+509	Jupiter	111.5	B	3.72 × 1.90
2003 Feb 1	0359+509	Jupiter	111.5	B	2.75 × 1.96
2003 Feb 3	0359+509	Jupiter	111.5	B	3.48 × 2.04

high- and low-velocity outflows from the embedded evolved star may also contribute significantly to the chemistry in the CSE. For example, within the high-velocity bipolar outflow, Ueta et al. (2001) discovered distinct near-IR "microstructures." They note that the positions of these microstructures occur in shocked regions where the molecular clumps are interfacing with the ambient circumstellar shell. Shocked regions also often trace areas of interesting interstellar chemistry that lead to the formation of complex molecular species. For example, Liu et al. (2002) detected formic acid (HCOOH) emission from shocked gas toward the Orion Compact Ridge. Also, Hollis et al. (2004) detected emission from propenal (CH_2CHCHO) and propanal (CH_3CH_2CHO) toward Sgr B2(N). The formation and widespread distribution of these species are most likely due to shocks in the Sgr B2(N) region that provided the energy necessary for the endothermic reactions to form these species and eventually distribute them into the gas phase. Thus, it appears that CRL 618 contains the physical conditions necessary to produce complex molecules.

Two recent surveys were performed toward CRL 618 using the *Infrared Space Observatory* (*ISO*) and the IRAM 30 m radio telescope (Cernicharo et al. 2001a, 2001b). These observations made the first detections in the circumstellar medium of the polyacetylenic chains C_4H_2 and C_6H_2 and the first detection of circumstellar benzene (C_6H_6). They also detected the infrared bands of NH_3 and C_2H_4 and made the first detection in the circumstellar medium of the methylpolyyenes CH_3C_2H and CH_3C_4H. Obviously, there is a rich chemistry available to form large carbon chain molecular species, including HC_3N and HC_5N (Fukasaku et al. 1994). Bujarrabal et al. (1988) compared the column densities of several molecular species measured toward CRL 618 to those measured toward other PPNe, specifically IRC +10216 and CRL 2688, as well as interstellar molecular clouds, specifically Orion A and TMC-1. What they found was that the abundances of many molecular species, including nitrogen-bearing species (e.g., HC_3N and HC_5N) and oxygen-bearing species (HCO^+ in particular), were more similar to the abundances found in the ISM rather than those in other PPNe. Furthermore, this was the first time HCO^+ was detected in a carbon-rich object. Thus, they suggested that CRL 618 was at a particular point in its evolution at which the chemistry occurring in the CSE was more similar to the chemistry in the ISM than to the chemistry of other PPNe (§ 4.5). There have also been detections of small oxygen-bearing molecules toward CRL 618, including CO, H_2O, and H_2CO (Cernicharo et al. 1989). However, there has not been any survey to fully investigate the extent of the chemistry present toward CRL 618 that may form larger oxygen-bearing molecules, although it appears to be the ideal environment to produce oxygen-bearing organic molecules, as well as other large molecular species.

Thus, to investigate whether the chemistry present toward CRL 618 can produce large oxygen-bearing organic molecules, we used the Berkeley-Illinois-Maryland Association (BIMA) Array[5] to carry out a large-molecule survey toward this region. Included in the survey were transitions of formic acid (HCOOH), acetic acid (CH_3COOH), methyl formate ($HCOOCH_3$), and acetaldehyde (CH_3CHO), as well as methyl cyanide (CH_3CN), cyanoacetylene (HC_3N), and cyanodiacetylene (HC_5N). The observations of these large molecules helped constrain not only the chemistry present toward CRL 618 but also the temperature and column density of large molecular species in the surrounding circumstellar environment.

2. OBSERVATIONS

The large-molecule survey took place from 2002 October to 2003 February using the B and C configurations of the BIMA Array. The minimum baseline for these observations was ∼8 m, and the maximum baseline was ∼150 m, providing angular resolutions of ∼2″–13″. Table 1 lists the observational parameters of our survey toward CRL 618. Column (1) lists the observation date. Column (2) lists the source used to calibrate the antenna-based gains, and column (3) lists the flux density calibrator. The absolute amplitude calibration of these sources is accurate to within ∼20%. We find a flux density of the source of 1.86 Jy at the continuum emission peak of our observations at 108 GHz, which is very similar to the flux density measured by Wyrowski et al. (2003) of 1.8 Jy with the IRAM 30 m radio telescope at 109.2 GHz. Column (4) lists the observing frequency of the upper sideband, and column (5) lists the array configuration of the observation. Finally, column (6) lists the corresponding beam size. To obtain the best signal-to-noise ratio at each observing frequency, all the data from the source with multiple tracks and in multiple arrays were inverted in *u-v* space. The resulting synthesized beam size (5″8 × 5″1, near 108 GHz) was determined by the region of densest *u-v* coverage, and the 1 σ rms noise level of the final maps was determined by selecting a region free from line and continuum emission. The passbands were calibrated automatically during data acquisition;[6] this method has been quite satisfactory and has not generated spurious features.

Table 2 lists the molecular parameters of the 44 transitions of the 15 molecular species searched for in our survey. Column (1)

TABLE 2

MOLECULAR LINE PARAMETERS

Species (1)	Transition (2)	Frequency[a] (MHz) (3)	$\langle S_{i,j}\mu^2\rangle$ (D²) (4)	E_u (K) (5)	Q_r (6)
C_6H[b]	$^2\Pi_{3/2}\,J=77/2-75/2\ f$	106,762.470(90)	1340.2	101.2	$89.8T$
^{34}SO[c]	2(3)–1(2)	106,743.374(18)	3.6	21.0	$2.9T$
$OC^{34}S$[d]	9–8	106,787.380(80)	4.6	25.7	$3.4T$
SO_2[b]	$27_{3,25}-26_{4,22}$	107,060.209(3)	8.3	370.5	$1.1T^{3/2}$
$MgNC$[b]	9–8	107,399.800(400)	245.2	25.9	$7.0T$
CH_3CN[e]	6(4)–5(4)	110,349.760(200)	51.0	132.3	$1.0T^{3/2}$
	6(3)–5(3)	110,364.470(100)	68.9	82.6	...
	6(2)–5(2)	110,374.986(120)	81.6	47.0	...
	6(1)–5(1)	110,381.376(120)	89.3	25.7	...
	6(0)–5(0)	110,383.494(120)	91.9	18.6	...
$(CH_3)_2O$[f]	$9_{1,8}-8_{2,7}\ AA$	106,775.679(80)	3.66	43.4	$91.6T^{3/2}$
	$9_{1,8}-8_{2,7}\ EE$	106,777.371(80)	3.66	43.4	...
	$9_{1,8}-8_{2,7}\ AE$	106,779.058(80)	3.66	43.4	...
	$9_{1,8}-8_{2,7}\ EA$	106,779.066(80)	3.66	43.4	...
CH_3CHO[b,g]	$3_{1,2}-2_{0,2}\ E$	107,887.477(1598)	0.02	8.07	$2.3T^{3/2}$
CH_3COOH[h]	$10_{*,10}-9_{*,9}\ E$	111,507.270(40)	54.8	30.5	$14.1T^{3/2}$
	$10_{*,10}-9_{*,9}\ A$	111,548.533(40)	54.8	30.5	...
CH_3C_3N[i]	27(6)–26(6)	111,503.905(3)	579.1	345.3	$8.7T^{3/2}$
	27(5)–26(5)	111,515.692(3)	588.3	262.8	...
	27(1)–26(1)	111,541.424(4)	608.4	82.7	...
	27(0)–26(0)	111,542.497(4)	609.2	75.2	...
CH_3CH_2OH[j]	$12_{7,6}-13_{6,7}$	111,510.340(31)	1.7	127.4	$6.5T^{3/2}$
	$12_{7,5}-13_{6,8}$	111,510.550(31)	1.7	127.4	...
	$8_{2,7}-8_{0,8}$	111,738.020(19)	0.1	35.3	...
$HCOOH$[k]	$5_{0,5}-4_{0,4}$	111,746.780(10)	10.0	16.2	$1.7T^{3/2}$
$HCOOCH_3$[l]	$9_{7,2}-8_{7,1}\ E$	110,525.598(32)	59.2	9.6	$12.4T^{3/2}$
	$9_{7,3}-8_{7,2}\ A$	110,535.182(28)	59.2	9.6	...
	$9_{7,2}-8_{7,1}\ A$	110,535.184(28)	59.2	9.6	...
	$9_{7,3}-8_{7,2}\ E$	110,535.955(26)	59.2	9.6	...
	$7_{2,6}-6_{1,5}\ E$	110,550.217(28)	19.0	1.4	...
	$7_{2,6}-6_{1,5}\ A$	110,560.053(30)	19.0	1.4	...
	$9_{1,8}-8_{1,7}\ E$	111,674.070(13)	22.8	28.9	...
	$9_{1,8}-8_{1,7}\ A$	111,682.224(13)	22.8	28.9	...
	$10_{1,10}-9_{0,9}\ E$	111,733.936(14)	3.8	30.3	...
	$10_{1,10}-9_{0,9}\ A$	111,735.329(15)	3.8	30.3	...
HC_3N[m]	$J=12-11\ (0,0,0,4)^0$	110,543.700(130)	169.4	1314.4	$13.7T$
	$J=12-11\ (0,0,0,4)^{2-}$	110,549.013(1594)	169.3	1314.4	...
	$J=12-11\ (0,0,0,4)^4$	110,554.377(42)	169.3	1314.4	...
	$J=12-11\ (0,1,0,3)^{1+}$	110,366.474(337)	169.0	994.4	...
HC_5N[n]	$J=40-39\ (0,0,0,1)^{1+}$	106,767.4842(44)	749.96	259.4	$15.7T$
	$J=40-39\ (0,0,0,3)^{1-}$	107,068.1920(300)	750.0	568.2	...
	$J=40-39\ (0,0,0,3)^{1+}$	107,254.3370(300)	750.0	568.4	...
	$J=40-39\ (0,0,0,4)^{4-}$	107,394.3161(50)	750.0	726.2	...
	$J=40-39\ (0,0,0,4)^{4+}$	107,394.3435(50)	750.0	726.2	...

[a] Errors are 2 σ.
[b] Pickett et al. (1998).
[c] Tiemann (1974).
[d] Maki (1974).
[e] Boucher et al. (1980).
[f] Groner et al. (1998).
[g] Bauder et al. (1976).
[h] Iluyshin et al. (2001).
[i] Müller et al. (2001).
[j] Lovas (1982).
[k] Willemot et al. (1980).
[l] Oesterling et al. (1999).
[m] Wyrowski et al. (1999); Yamada & Creswell (1986).
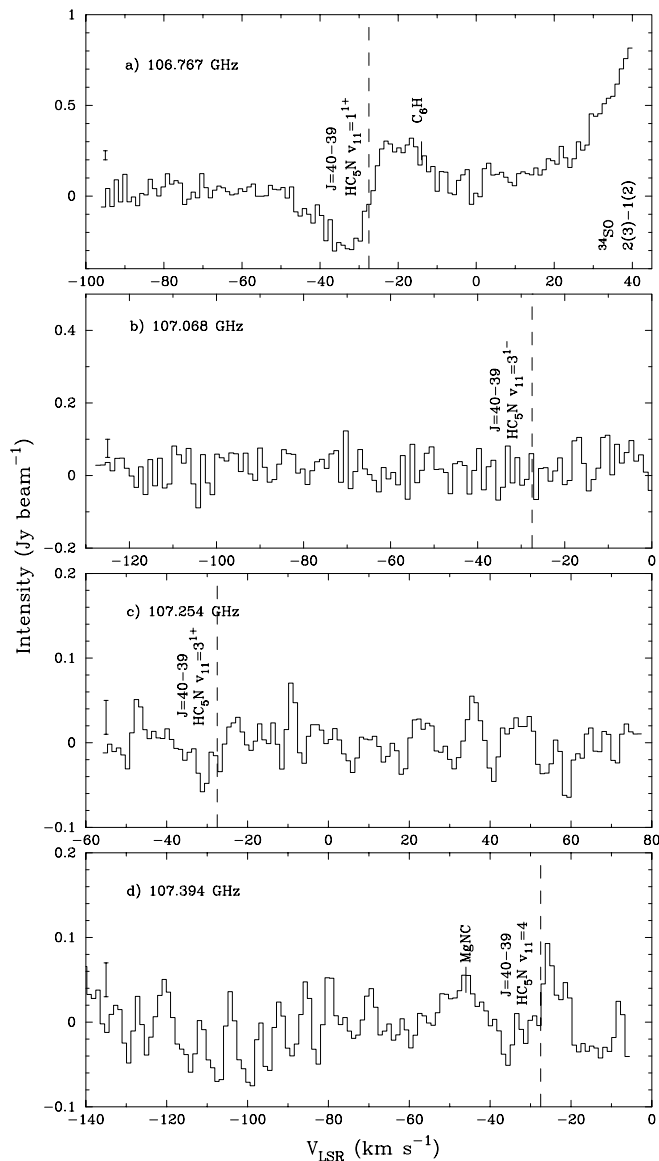[n] Yamada et al. (2004); Müller et al. (2001).

FIG. 1.—Spectra of the four transitions of vibrationally excited HC$_5$N located in the passbands of our survey. (a) First detection the HC$_5$N $J = 40$–39, (0, 0, 0, 1)$^{1+}$ transition toward CRL 618 seen in absorption and emission. The emission peaks near a v_{LSR} of -24 km s^{-1}. The spectral line label in the upper left of each panel is the rest frequency of each HC$_5$N transition for a v_{LSR} of -27.5 km s^{-1}. The dashed line is centered on the v_{LSR} of CRL 618 (-27.5 km s^{-1}). Near 40 km s^{-1} we begin to detect the ^{34}SO 2(3)–1(2) transition in emission. We also label the location of the C$_6$H $^2\Pi_{3/2} J = 77/2$–75/2 f transition. The 1 σ rms noise level is ~40 mJy beam^{-1} (vertical bar at the left of each spectrum). (b) Passband containing the HC$_5$N $J = 40$–39, (0, 0, 0, 3)$^{1-}$ transition toward CRL 618. No spectral feature is detected beyond the 1 σ rms noise level. (c) Passband containing the HC$_5$N $J = 40$–39, (0, 0, 0, 3)$^{1+}$ transition toward CRL 618. No spectral feature is detected beyond the 1 σ rms noise level. (d) Passband containing the HC$_5$N $J = 40$–39, (0, 0, 0, 4) transition toward CRL 618. We also label the location of the MgNC $N = 9$–8 transition. No spectral feature is detected beyond the 1 σ rms noise level; however, the MgNC transition is beginning to be resolved out of the noise (§ 4.4).

lists the species; Column (2) lists the transition. Column (3) lists the calculated rest frequency and its 2 σ standard deviation. Column (4) lists the product of the line strength and the square of the relevant dipole moment, and column (5) lists the upper state energy level of each transition. Finally, the estimated rotational partition functions for each molecular species are given in column (6). The spectral windows containing these transitions had a bandwidth of 50 MHz and were divided into 128 channels for a spectral

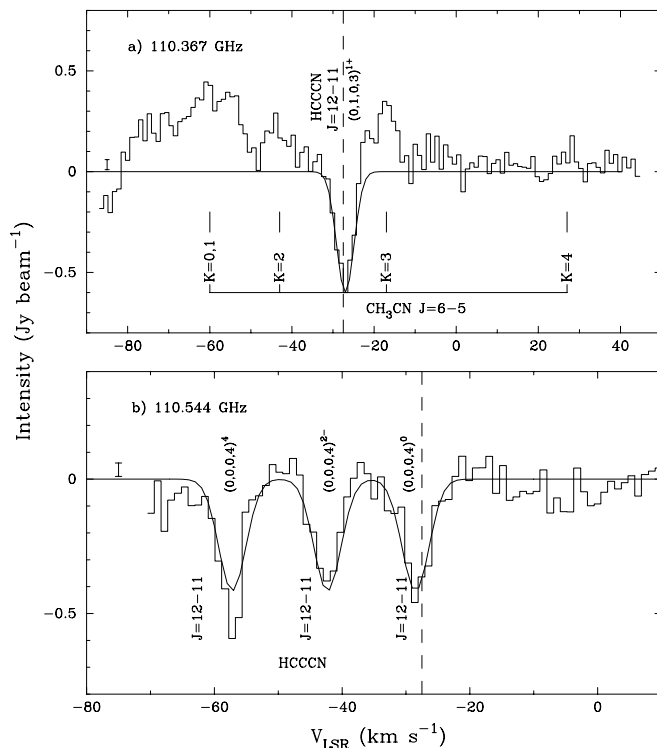FIG. 2.—Spectra of the detected transitions of CH$_3$CN and HC$_3$N found from our survey toward CRL 618. (a) First detection of the $J = 6$–5 rotational transitions of CH$_3$CN seen entirely in emission. Between the $K = 2$ and 3 lines of CH$_3$CN lies the $J = 12$–11 (0, 1, 0, 3)$^{1+}$ vibrational transition of HC$_3$N seen in absorption. The measured v_{LSR} of the absorption trough of HC$_3$N is -27.5 km s^{-1}. The spectral line label in the upper left of the panel is the rest frequency of the HC$_3$N transition. The 1 σ rms noise level is ~40 mJy beam^{-1} (vertical bar at the left of each spectrum). (b) Spectrum of three vibrationally excited transitions of HC$_3$N. Each of these transitions lies at a v_{LSR} of -27.5 km s^{-1}. The spectral line labels located in the upper left of each panel correspond to the rest frequency of the HC$_3$N $J = 12$–11 (0, 0, 0, 4)^0 transition.

resolution of 0.39 MHz per channel. All data were combined, imaged, and self-calibrated using the MIRIAD software package (Sault et al. 1995). The 1 σ rms noise level of the final maps was used to set upper limits on the column densities of the undetected molecular species searched for in our survey (§ 4.4).

3. RESULTS

Figure 1 shows the four transitions of vibrationally excited HC$_5$N located in the passbands of our survey. The HC$_5$N transitions and corresponding rest frequencies were taken from a new survey by Yamada et al. (2004) and the Cologne Database for Molecular Spectroscopy (Müller et al. 2001). In Figure 1a we show the first interferometric detection of vibrationally excited ($v_{11} = 1$) HC$_5$N toward CRL 618. The spectral line labels located in the upper left of each panel correspond to the rest frequency of each HC$_5$N transition for a v_{LSR} of -27.5 km s^{-1} (dashed line). The 1 σ noise level is seen at the left of each panel. The classic P Cygni line profile indicates that HC$_5$N is present in an expanding envelope of material. Also included in Figure 1a are the spectral line labels of C$_6$H and ^{34}SO. These features will be discussed in more detail (§§ 4.4 and 4.5). Figures 1b–1d show the spectra of higher vibrational transitions ($v_{11} = 3$ and 4) that were not detected beyond our 1 σ detection limit. From these nondetections, we were able to set an upper limit on the temperature of this species in this region. Finally, in Figure 1d, we label the location of MgNC. The nondetection of this feature will also be discussed in more detail (§ 4.4).

TABLE 3
Line Detections

Frequency (MHz) (1)	Species (2)	Transition (3)	v_{LSR} (km s^{-1}) (4)	$\int \Delta I\, dv$ (Jy beam^{-1} km s^{-1}) (5)
106,767.4842(44).............	HC$_5$N	$J = 40$–39 $(0, 0, 0, 1)^{1+}$	-24	4.74(1.9)
. . .	. . .	. . .	-34	-4.15(1.7)
106,743.374(18)...............	^{34}SO	2(3)–1(2)	. . .	a
110,349.760(200).............	CH$_3$CN	6(4)–5(4)	-27.5	0.58(42)
110,364.470(100).............	CH$_3$CN	6(3)–5(3)	-27.5	2.77(18)
110,366.742(337).............	HC$_3$N	12–11 $(0, 1, 0, 3)^{1+}$	-27.5	-2.69(30)
110,374.986(120).............	CH$_3$CN	6(2)–5(2)	-27.5	1.85(17)
110,381.376(120).............	CH$_3$CN	6(1)–5(1)	. . .	b
110,383.494(120).............	CH$_3$CN	6(0)–5(0)	-27.5	7.63(24)[b]
110,543.508(130).............	HC$_3$N	12–11 $(0, 0, 0, 4)^0$	-27.5	-1.56(3)
110,550.328(1594)............	HC$_3$N	12–11 $(0, 0, 0, 4)^{2-}$	-27.5	-1.38(3)
110,554.742(42)................	HC$_3$N	12–11 $(0, 0, 0, 4)^4$	-27.5	1.92(3)[c]

[a] Because we did not see the line peak, no attempt was made to fit this transition.

[b] Because the $K = 0$ and 1 components could not be fitted with separate Gaussians, a one-Gaussian fit was applied to both lines.

[c] This line may be blended with the $15_{4,2}$–$14_{5,2}$ transition of c–C$_3$H$_2$ at 110.558(9) GHz (Pickett et al. 1998).

Figure 2 shows the spectra of the CH$_3$CN and vibrationally excited HC$_3$N detected in our survey. Figure 2a shows the first detection of the $J = 6$–5 rotational transitions of CH$_3$CN. All the CH$_3$CN transitions are seen in emission. Between the $K = 2$ and 3 lines of CH$_3$CN lies the $J = 12$–11, $(0, 1, 0, 3)^{1+}$ vibrational transition of HC$_3$N seen in absorption. The measured v_{LSR} of the absorption trough is -27.5 km s^{-1}, which is consistent with previous detections of vibrationally excited HC$_3$N (Wyrowski et al. 2003). Finally, Figure 2b shows the spectrum of three vibrationally excited transitions of HC$_3$N. Once again, each of these transitions lies at a v_{LSR} of -27.5 km s^{-1}. The spectral line labels located at upper left in Figures 2a and 2b correspond to the rest frequency of the HC$_3$N $J = 12$–11, $(0, 1, 0, 3)^{1+}$ and the HC$_3$N $J = 12$–11, $(0, 0, 0, 4)^0$ transitions,[7] respectively. Table 3 lists the molecular species that were detected toward CRL 618 at or near the systemic velocity (-27.5 km s^{-1}). Least-square Gaussian fits were made for each spectral line to obtain the radial velocities and integrated line intensities for the detected transitions. In Table 3, column (1) lists the calculated rest frequencies of the identified species. Columns (2) and (3) list the molecular species and associated transitions, respectively. Column (4) lists the v_{LSR} corresponding to the emission or absorption components of each spectral feature. Finally, column (5) lists the fitted integrated line intensity of each detected transition and the associated 1 σ uncertainty.

Figure 3 shows the HC$_5$N velocity channel maps toward CRL 618. The spectral line channel maps displayed are a combination of the B- and C-array data. The v_{LSR} intervals are indicated in km s^{-1} units at the top right of each panel. The synthesized beam of $5\farcs8 \times 5\farcs1$ is shown at the bottom left of each velocity channel map. The lowest contour plotted is 0.08 Jy beam^{-1} which corresponds to 2 σ. The absorption peaks near a v_{LSR} of -34 km s^{-1}, and the emission peaks near -24 km s^{-1}. Both the absorption and emission peaks are coincident with the high-resolution B-array 3 mm continuum shown in the bottom right panel of the figure (synthesized beam of $3\farcs0 \times 1\farcs9$). Thus, it is apparent from both the P Cygni profile and velocity channel maps that HC$_5$N

is contained in an expanding envelope and not in the bipolar outflows.

Figure 4 shows the HC$_3$N velocity channel maps toward CRL 618. As in Figure 3, the data displayed are a combination of the B- and C-array data, and the v_{LSR} intervals are indicated at top right in each panel. In this case, we see no emission features of HC$_3$N. This is not unexpected because all the high-energy, high vibrational state transitions (i.e., $v_5 = 1$ and $v_7 = 3$) detected by Wyrowski et al. (2003) were seen primarily in absorption. The transitions detected in our survey were at a higher vibrational state ($v_7 = 3$ or 4) than the transitions of the Wyrowski et al. (2003) survey, but the upper state energy levels were comparable to some of the higher energy transitions detected in their survey. In contrast, the ground state and first vibrational states in the Wyrowski et al. (2003) survey were seen primarily in emission. Once again, we see that the absorption is coincident with the 3 mm continuum, and presumably all the vibrationally excited HC$_3$N is contained in the CSE.

Finally, we note that we did not detect any emission or absorption features from any of the other molecular species listed in Table 2 beyond our 1 σ detection limit. These include all the oxygen-bearing organic molecules, as well as CH$_3$C$_3$N, C$_6$H, and all the smaller molecular species. However, it does appear that we are starting to detect the $N = 9$–8 transition of MgNC in Figure 1d. Higher signal-to-noise ratio interferometric observations are necessary to confirm this detection. Based on the 1 σ detection limit, we were able to place upper limits on the species that were not detected. All column densities and upper limits are listed in Table 4 (§ 4.4). In § 4.5 we discuss these upper limits, along with the predicted fractional abundances based on the gas-phase formation models of Woods et al. (2003) and in the UMIST database (Le Teuff et al. 2000).

4. ANALYSIS AND DISCUSSION

One of the most important physical parameters to determine in either an interstellar or circumstellar environment is the total beam-averaged column density of a molecular species. There are three primary procedures used in calculating the total beam-averaged column density of a particular molecular species, each of which is described in detail in Remijan et al. (2004b). For our purposes, we use the rotational temperature diagram method

___
[7] The notation given for the vibrational excited transitions of HC$_3$N is defined as $(v_4, v_5, v_6, v_7)^l$, where v is the vibrational quantum number and l is the l-type–doubling quantum number (Thorwirth et al. 2003).
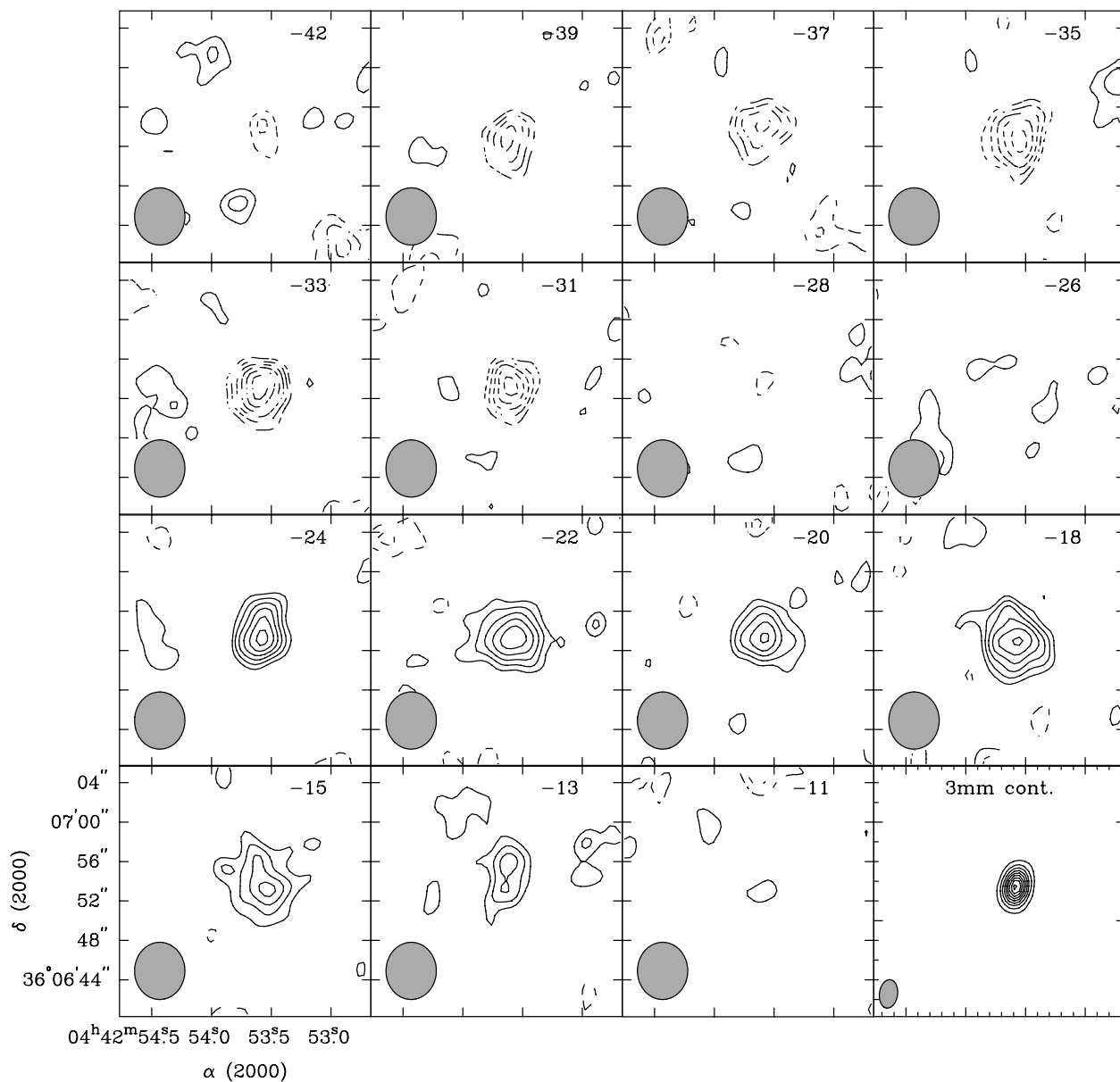
FIG. 3.—HC$_5$N velocity channel maps toward CRL 618. The data displayed are a combination of those from the B- and C-array data. The LSR velocities of the absorption and emission features are indicated in km s^{-1} at the top right of each panel. The contour level ranges are -0.24, -0.20, -0.16, -0.12, -0.08, 0.08, 0.12, 0.16, 0.20, 0.24 and 0.28 Jy beam^{-1}. The synthesized beam of 5″8 × 5″1 is shown at the lower left of each panel. *Bottom right*: Continuum emission at 3 mm toward CRL 618 in the BIMA B array. The synthesized beam of 3″0 × 1″9 is shown at lower left, The continuum emission peaks at an intensity of 1.86 Jy beam^{-1} at a frequency near 108 GHz.
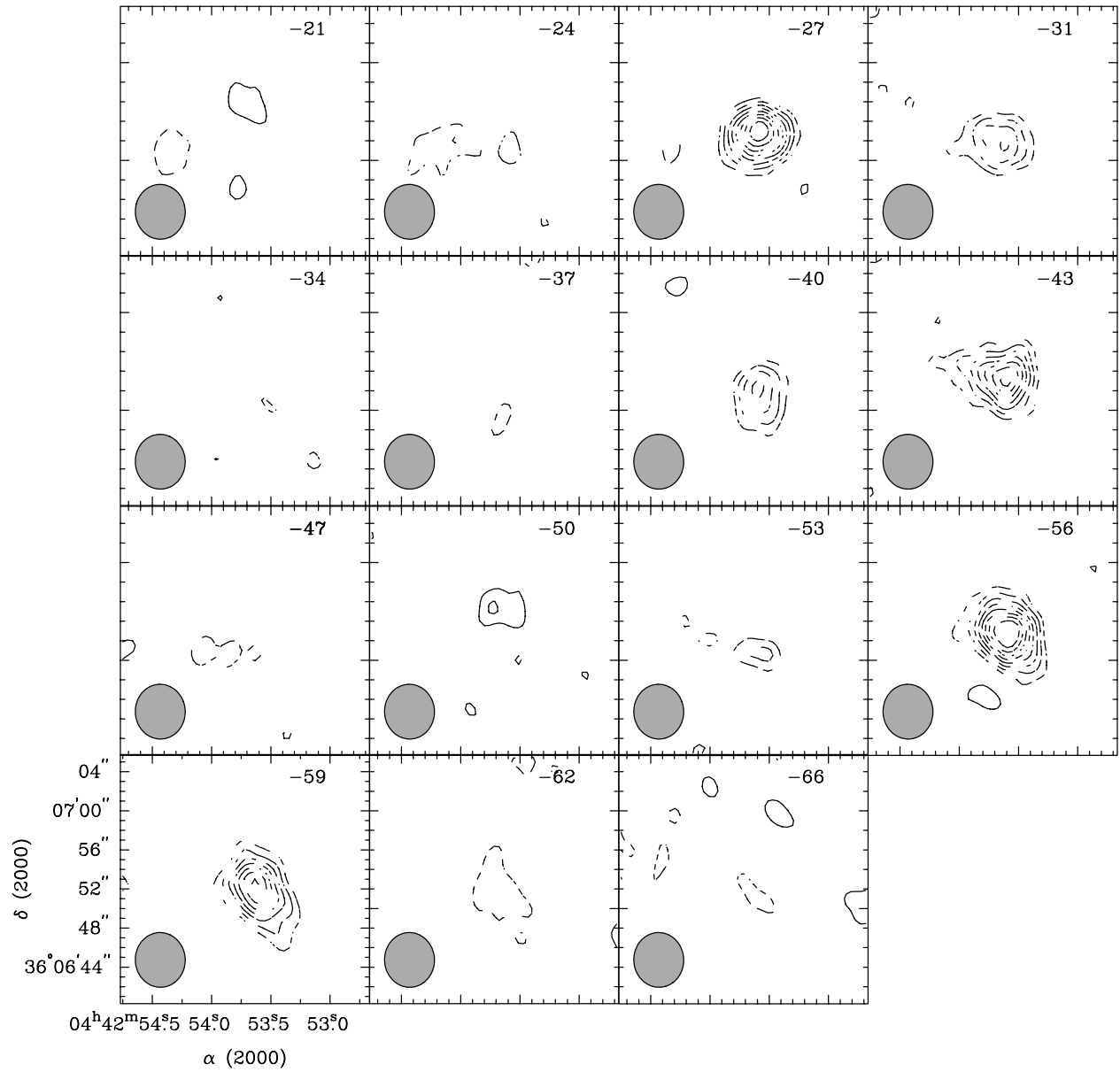
F$_{IG}$. 4.—HC$_3$N $v_7 = 4$ velocity channel maps toward CRL 618. The data displayed are a combination of those from the B- and C-array data. The panel labels and beam sizes are the same as in Fig. 3. The contour level ranges are -0.36, -0.32, -0.28, -0.24, -0.20, -0.16, -0.12, -0.08, 0.08, and 0.12 Jy beam^{-1}.

TABLE 4
COLUMN DENSITIES

Species (1)	Frequency (MHz) (2)	$N_{\rm tot}$ (cm^{-2}) (3)	X(H$_2$) (4)
Detections			
HC$_5$N[a]	106,767.484	9.9×10^{14}	7.6×10^{-9}
HC$_3$N......................	[b]	$4.7\,(6) \times 10^{17}$	$3.6\,(5) \times 10^{-6}$
CH$_3$CN	[b]	$3.2\,(3) \times 10^{14}$	$2.4\,(3) \times 10^{-9}$
Upper Limits			
C$_6$H	106,762.470	2.5×10^{13}	1.9×10^{-10}
OC^{34}S	106,787.380	1.2×10^{14}	9.1×10^{-10}
SO$_2$..........................	107,060.209	1.0×10^{16}	7.8×10^{-8}
MgNC	107,399.800	4.4×10^{12}	3.4×10^{-11}
HCOOCH$_3$	110,550.217	1.1×10^{16}	8.5×10^{-8}
(CH$_3$)$_2$O.................	106,777.371	1.0×10^{17}	7.9×10^{-7}
CH$_3$CHO	107,887.477	1.4×10^{17}	1.1×10^{-6}
CH$_3$COOH	111,548.533	3.5×10^{14}	2.7×10^{-9}
CH$_3$C$_3$N.................	111,542.497	3.3×10^{13}	2.5×10^{-10}
CH$_3$CH$_2$OH...........	111,738.020	9.4×10^{16}	7.3×10^{-7}
HCOOH	111,746.780	2.0×10^{14}	1.5×10^{-9}

[a] Column density based on the emission-line detection (§ 4.3).
[b] All lines were used to calculate the total column density of this molecule.

(RTDM) for the CH$_3$CN and HC$_5$N emission and assume local thermodynamic equilibrium (LTE) for all other molecular species. From Remijan et al. (2003), the total beam-averaged column density is given as

$$N_T = 2.04 C_\tau \frac{\int \Delta I \, dv}{\theta_a \theta_b} \frac{I(T_e)}{I(T_e) - I_b} \frac{Q_{\rm rv} e^{(E_u/T_e)}}{\nu^3 \langle S_{ij}\mu^2 \rangle} \times 10^{20} \ \rm cm^{-2}$$
$$= C_\tau N_T^{\rm thin} \ \rm cm^{-2}, \tag{1}$$

where N_T is the total column density for any optical depth and $N_T^{\rm thin}$ is the total column density for the optically thin case, C_τ is the optical depth correction factor from Goldsmith & Langer (1999), $\int \Delta I \, dv$ (in Jy beam^{-1} km s^{-1}) is the integrated line intensity given in Table 3, θ_a and θ_b are the FWHM beam sizes (in arcseconds), $I(T_e)$ is the specific intensity of the source at T_e (in Jy beam^{-1}), I_b is the specific intensity of the total background continuum contribution (in Jy beam^{-1}), and $Q_{\rm rv}$ is a combination of the rotational and vibrational partition functions. The vibrational part of the partition function needs to be applied to both the HC$_5$N (Müller et al. 2001) and the the HC$_3$N (Wyrowski et al. 2003) column density calculations. E_u is the upper state energy level (in K), T_e is the rotational temperature (in K), ν is the rest frequency (in GHz), and $S_{ij}\mu^2$ is the product of the total torsional-rotational line strength and the square of the electric dipole moment (debye^2).

4.1. Methyl Cyanide (CH$_3$CN)

Methyl cyanide (CH$_3$CN) has been used as an excellent tracer of the physical and chemical conditions toward high-mass star-forming regions of the ISM (Remijan et al. 2004b; Sutton et al. 1986). CH$_3$CN is a symmetric top molecule whose properties make it an ideal probe of kinetic temperature and column density. In a symmetric top, the rotational levels are labeled by J, the total angular momentum quantum number, and K, the quantum number for the projection of the angular momentum vector along the
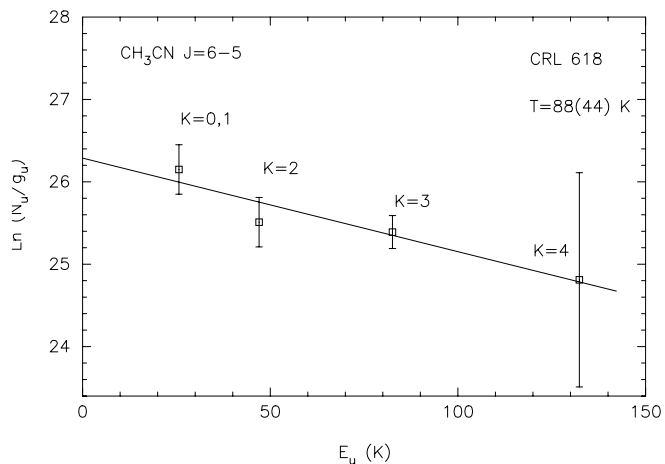

FIG. 5.—Rotational temperature diagram for the observed CH$_3$CN transitions toward CRL 618. *Ordinate*, ln (N_u/g_u); *abscissa*, E_u(in K). The least-squares fit is shown as a solid line. The resulting rotational temperature is 88 (44) K in a beam size of $5''.8 \times 5''.1$.

symmetry axis (Cummins et al. 1983). By selection rules, radiative transitions do not change the value of K. However, collisional transitions are permitted across K ladders. Therefore, the population of one K ladder relative to another is largely determined by collisions and hence is closely related to the kinetic temperature and density (Solomon et al. 1971). The first reported detection of CH$_3$CN toward CRL 618 was by Bujarrabal et al. (1988) using the IRAM 30 m radio telescope. Also with the IRAM 30 m, Guelin & Cernicharo (1991) used several millimeter transitions of CH$_3$CN to examine the physical conditions toward IRC +10216. From their observations, they found a rotation temperature of $T_{\rm rot} = 16$ K and a column density of 6×10^{12} cm^{-2} toward IRC +10216 (Guelin & Cernicharo 1991). Figure 5 shows the results of the RTDM toward CRL 618 using the $J = 6$–5 transitions. Because the $K = 0$ and 1 transitions are severely blended, we could not resolve the lines into two separate Gaussians; thus, we included the pair as one point on the rotational temperature diagram by separating the intensities by their appropriate statistical weights and then averaging. Using the procedures outlined in Remijan et al. (2004b), we found a best-fit rotational temperature of 88 (44) K and a total beam-averaged column density of $3.2(3) \times 10^{14}$ cm^{-2}. Assuming an H$_2$ column density of $\sim 1.3 \times 10^{23}$ cm^{-2} (Woods et al. 2003), we find a fractional abundance of $X_{\rm CH_3CN} = 2.4(3) \times 10^{-9}$. This value is very close to the predicted peak value of $\sim 10^{-8}$ from the Woods et al. (2003) model at a radial distance of $\sim 9.1 \times 10^{15}$ cm from the exciting star. Thus, it is clear from our observations that CH$_3$CN appears to reside in the outer regions of the expanding envelope. Furthermore, transitions of vibrationally excited CH$_3$CN $v_8 = 1$ are below our 1 σ detection limit, which again may imply that CH$_3$CN exists in the outer envelope.

4.2. Cyanoacetylene (HC$_3$N)

Cyanoacetylene (HC$_3$N) is a carbon chain molecule that has been extensively studied toward CRL 618 in both the ground and excited vibrational states (see, e.g., Pardo et al. 2004; Wyrowski et al. 2003 and references therein). So, from our data, we were able to check the previously measured physical conditions and help further constrain the physical and chemical models of CRL 618. In Figure 2, we show the detections of four vibrationally excited transitions of HC$_3$N. Also shown in these spectra are the best-fit modeled spectra to the data (*solid line*). To calculate the best-fit

spectra, we used the spectral line parameters given in Table 2 and used an FWHM line width of $\Delta v = 5$ km s^{-1} based on the fits in Table 3. Models were constructed using the temperature and upper state column density as input parameters. We varied the temperature between 400 and 600 K and the upper state column density between 10^{16} and 10^{18} cm^{-2}. We then calculated the χ^2 between the model and the data and found the minimum χ^2. The best-fit models (*solid lines*) are shown in Figure 2 for a temperature of 580 (150) K and a total HC$_3$N beam-averaged column density of $4.7(6) \times 10^{17}$ cm^{-2}. The errors given for the temperature and total column density are 3 σ errors based on the fit, thus giving a 99% confidence interval. The only line that does not seem to fit the model very well is the $J = 12$–11 $(0, 0, 0, 4)^4$ transition at 110.555 GHz (Table 2). This line may be blended with the $15_{4,2}$–$14_{5,2}$ transition of c–C$_3$H$_2$ at 110.558(9) GHz (Pickett et al. 1998) or possibly a transition from another unknown circumstellar species. The values of $T_{\rm rot}$ and N_T are very similar to the values determined by Wyrowski et al. (2003) of $T = 520(80)$ K and a total HC$_3$N column density between $(3-6) \times 10^{17}$ cm^{-2}. To find the total HC$_3$N column density, we need to include the vibrational part of the partition function. Using Figure 9 in Wyrowski et al. (2003) and a temperature of 580 K, we find $Q_{\rm rv} = 1.8 \times 10^5$. Also in equation (1) we need to account for the optical depth and the intensity of the background continuum. For the HC$_3$N lines, we find $\tau = \ln (T_c/T_c - T_L) = 0.25$, which gives an optical depth correction factor of $C_\tau = 1.13$, and if we use the continuum temperature and the excitation temperature of 580 K, the column density correction due to $I(T_{\rm ex})/[I(T_{\rm ex}) - I_b]$ is ~ 1.06, which gives a total correction of ~ 1.20 for a temperature of 580 K. Assuming an H$_2$ column density of $\sim 1.3 \times 10^{23}$ cm^{-2} (Woods et al. 2003), we find a fractional abundance of $X_{\rm HC_3H} = 3.6(5) \times 10^{-6}$, which matches that of the models of Woods et al. (2003). The average value of the HC$_3$N fractional abundance in the envelope predicted by the model is $\sim 10^{-6}$, and the model predicts a peak value of 1.6×10^{-6} at a radial distance of $\sim 10^{16}$ cm from the central star. Thus, it appears that the models are predicting the relative abundance of this species very well toward CRL 618.

4.3. *Cyanodiacetylene* (HC$_5$N)

The first reported detection of HC$_5$N in a PPN was by Winnewisser & Walmsley (1978) toward IRC +10216. They observed the $J = 9$–8 rotational transition near 24 GHz. From their observations, they found the HC$_5$N emission to be quite extended over their $40''$ beam and measured an HC$_5$N column density of 4×10^{14} cm^{-2}. However, they did not detect any emission from the $v_{11} = 1$ vibrational mode. These observations were later followed up by Jennings & Fox (1982), who determined an HC$_5$N rotational temperature of 13^{+12}_{-4} K, which was in agreement with the determined HC$_3$N rotational temperature of 12 K measured at the time. The first detection of HC$_5$N in CRL 618 was by Bujarrabal et al. (1988). In this case, they assumed the HC$_5$N emission to be much smaller than their beam of $\sim 15''$. From that, they found an HC$_5$N rotational temperature of ~ 81 K. Since then, several other transitions of HC$_5$N have been observed toward other PPNe (see, e.g., Fukasaka et al. 1994). The first detection of vibrationally excited transitions of HC$_5$N reported in CRL 618 was by Thorwirth (2001). Later observations followed by Cernicharo et al. (2001b) and Wyrowski et al. (2003). However, ours are the first data of vibrationally excited HC$_5$N taken with an interferometer and the first maps of vibrationally excited HC$_5$N toward CRL 618. In Figure 1, we showed the first interferometric detection of the $J = 40$–39, $v_{11} = 1$ transition of HC$_5$N. No higher vibrational states ($v_{11} = 3$ or 4) were detected (Figs. 1b–1d). However, from the 1 σ noise

levels, we were able to plot the upper limits on a rotational temperature diagram of HC$_5$N. Plotting these data on a rotational temperature diagram, we were able to determine an upper limit on the HC$_5$N rotational temperature of $T_{\rm rot} = 114$ K. Using the measured vibrationally excited partition function from Müller et al. (2001) for HC$_5$N, we were able to calculate the total rotational-vibrational HC$_5$N partition function for 114 K. We find $Q_{\rm rv} \simeq 950$. From the rotational temperature diagram, we find a total beam-averaged column density of HC$_5$N of $\sim 10^{15}$ cm^{-2} and a fractional abundance of $X_{\rm HC_3H} = 7.6 \times 10^{-9}$. This column density is about an order of magnitude lower than the predicted value of 1.7×10^{16} cm^{-2} from the Woods et al. (2003) model. However, the column density is in the range of measured values toward this source from previous observations (Fukasaku et al. 1994; Cernicharo et al. 2001b).

Also, looking at the velocity channel maps in Figure 3, we see that the HC$_5$N emission is coincident with the 3 mm continuum and that no HC$_5$N emission is seen in the bipolar outflow above our 3 σ detection limit cutoff. The classic P Cygni line profile indicates a spherically symmetric expansion with an expansion velocity of ~ 5–7 km s^{-1}. The slow expansion velocity would occur at the outer edges of the envelope as the expanding material begins to interact with the remnant AGB wind. Also, the expansion velocity of HC$_5$N is close to the measured expansion velocity of HC$_3$N (~ 10 km s^{-1}) found by Pardo et al. (2004), and it matches the expansion velocity used by Woods et al. (2003) in their formation models. Thus, from the spectral line profile and mapping data it appears that HC$_5$N is found in the extended CSE.

To summarize, all the detected species are found in the extended envelope. In the case of CH$_3$CN, the observed transitions are low in upper state energy and are optically thin. Thus, we are probing the gas in the very extended envelope and should see only emission features. On the other hand, the HC$_3$N transitions have high upper state energies. The gas sampled in this case must lie deeper in the envelope, where the column density is high, which leads to a high opacity, and the lines are seen primarily in absorption. Transitions of HC$_3$N at a lower energy state with respect to the transitions we observed are seen by other authors in emission and as P Cygni profiles. This implies that these authors are sampling the outer envelope where the gas is at a lower temperature but the column density is high enough that there are competing effects of emission and absorption (see, e.g., Pardo et al. 2004). Finally, for HC$_5$N, the temperature implies that the gas resides in the outer envelope, intermediate between the vibrational HC$_3$N and lower energy CH$_3$CN transitions, and that the column density is high enough that, once again, there are competing effects of emission and absorption. The hypothesis based on the formation models of each species (Woods et al. 2003) is that CH$_3$CN, HC$_3$N, and HC$_5$N are probably contained throughout the CSE of CRL 618. To fully investigate that assumption, observations of transitions that sample a wide range of upper state energy levels of each species are necessary.

4.4. *Column Density Upper Limits of the Remaining Molecular Species*

Of the remaining species listed in Table 2, we detected emission from ^{34}SO only (Fig. 1a). Because this line was near the edge of the spectral window, we were not able to make a Gaussian fit or a calculation of the total ^{34}SO beam-averaged column density. However, this is the first detection of this isotopic species of SO in a PPN. Further observations of ^{34}SO and ^{32}SO will be needed to determine the isotopic ratio and compare the column densities with those of other detected O-bearing species, including CO and H$_2$O toward CRL 618 (Herpin & Cernicharo 2000).

We also note that we did not reliably detect any emission from the $N = 9-8$ transition of magnesium isocyanide (MgNC). This species was recently detected using the Arizona Radio Observatory (ARO) 12 m and the IRAM 30 m telescopes via five rotational transitions at 95.4, 131.2, 143.2, 151.1, and 167.0 GHz. The column density of MgNC from that survey was found from a rotational temperature diagram to be 2.4×10^{12} cm^{-2} with a $T_{\rm rot} = 21$ K (Highberger & Ziurys 2003). They note that the derived rotational temperature is consistent with the kinetic temperature of ~ 50 K (Herpin et al. 2002). Using this column density, we can predict the expected line intensity for our observations. Using a rotational temperature of 21 K, we predict an intensity of ~ 0.035 Jy beam^{-1} for our BIMA observations. If the temperature is closer to the CH$_3$CN temperature of 88 K, the predicted intensity drops to ~ 0.022 Jy beam^{-1}. The average rms noise of the combined B- and C-array data set containing the MgNC transition is ~ 0.04 Jy beam^{-1}. Thus, even with the highest predicted line intensity, we would have detected this transition only at the $\sim 1\ \sigma$ level. In Figure 1d, we labeled the position of the MgNC transition, and it appears the line is beginning to be resolved out of the noise. However, higher signal-to-noise ratio interferometric observations are necessary to claim this as a detection.

No other molecular species were detected toward CRL 618 beyond the $1\ \sigma$ detection limit. However, we were able to set upper limits on the column densities of those species based on the $1\ \sigma$ rms noise level (~ 0.04 Jy beam^{-1}) and an average line width of ~ 5 km s^{-1}, assuming a temperature of 88 K found from the CH$_3$CN data. Table 4 summarizes the column densities of all molecular species, including upper limits. Column (1) lists the molecular species observed toward CRL 618. Column (2) lists the frequency of the transition used to calculate the upper limit on the total column density (MHz). Using equation (1), an average beam of 25 arcsec^2, and the spectroscopic parameters and partition functions in Table 2, we were able to calculate the total beam-averaged column densities of each molecular species. Column (3) lists the total beam-averaged column density (in cm^{-2}). Finally, column (4) lists the fractional abundance of each molecular species with respect to H$_2$, assuming an H$_2$ column density of 1.3×10^{23} cm^{-2}.

4.5. Formation and Detection of Oxygen-bearing Organic Biomolecules in Proto−Planetary Nebulae

Our detections of CH$_3$CN, HC$_3$N, and HC$_5$N strongly suggest that the chemistry present toward CRL 618 is conducive to producing large carbon chain molecules and that the formation models that predict the abundance of these species also match the measured abundances very well. The only large carbon chain molecule that was predicted to be present in a large abundance toward CRL 618 but was not detected was C$_6$H. Woods et al. (2003) predict a total column density of 2.5×10^{15} cm^{-2}, and our measured upper limit was 2 orders of magnitude lower, at 2.5×10^{13} cm^{-2}. Also, there is no formation model that takes into account methylcyanoacetylene (CH$_3$C$_3$N), and our measured upper limit is 3.3×10^{13} cm^{-2}. However, the models of Woods et al. (2003) predict the column densities of CH$_3$C$_4$H and C$_6$H$_5$CN, which are presumed to be more complex species than either C$_6$H or CH$_3$C$_3$N, to be 1.5×10^{15} cm^{-2}. Thus, if the formation models are correct, we should have easily detected C$_6$H. If the predicted column density of CH$_3$C$_3$N is similar to either CH$_3$C$_4$H or C$_6$H$_5$CN, we should have also easily detected CH$_3$C$_3$N. The fact that neither species was detected beyond our $1\ \sigma$ detection limit implies that the calculated upper limit of $\sim 10^{13}$ cm^{-2} for both C$_6$H and CH$_3$C$_3$N must be taken into account in future formation models.

In addition to large carbon chain molecules, there have been several detections of simple, singly oxygenated species detected in the CSE and in the bipolar outflows of CRL 618. These molecules include CO, H$_2$O, H$_2$CO (Cernicharo et al. 1989), and HCO$^+$ (Bujarrabal et al. 1988). The hypothesis of Bujarrabal et al. (1988) was that the CSE was at a particular point in its evolution at which the opacity was low enough to allow UV photons from the central star to act on existing molecules in the CSE. In fact, only PPNe younger than ~ 300 yr are seen to be molecule-rich. In older PPNe, such as NGC 2346 and the Red Rectangle, photodissociation by UV photons can explain the lack of molecular emission seen toward these objects. In contrast, objects younger than CRL 618, including CRL 2688 and IRC +10216, show an abundance of molecular emission from large carbon chain species, such as HC$_3$N; however, the chemistry involving photodissociation has not evolved to the point of forming larger molecules from simply oxygenated species. CRL 618 is unique in that it has evolved enough to begin an interesting circumstellar chemistry but not to the point at which a large number of molecules are being quickly dissociated. The high abundance of HCO$^+$ with respect to younger objects supports this hypothesis. In fact, the abundance of many oxygen-bearing molecules in CRL 618 is very similar to the abundances found in oxygen-rich PPNe, including OH 231.8+4.2. HCO$^+$, and other small singly oxygenated molecules, including atomic oxygen (Herpin & Cernicharo 2000), are used in gas chemistry models to produce more complex and organic molecules of biological importance.

The nondetections of very favorable transitions of oxygen-bearing organic molecules such as HCOOH, HCOOCH$_3$, and CH$_3$COOH, however, imply that the chemistry of PPNe may not be conducive to form large organic molecules of biological interest (biomolecules). In fact, the only biomolecules that have been detected toward a PPN are formaldehyde (H$_2$CO; Cernicharo et al. 1989), toward CRL 618, and, in a tentative but unverified detection, methanol (CH$_3$OH), toward IRC +10216 (Latter & Charnley 1996). Numerous chemical models have been used to try to explain the formation and measured abundances of oxygen-bearing organic molecules in the ISM and CSE. These models include many different types of energetics, including shocks and thermal heating to drive the predicted chemistry. For our purposes, we include only a brief overview of some models and how they may apply to CSEs.

In the case of forming CH$_3$OH and H$_2$CO in a CSE, shock chemistry is invoked to explain the formation of H$_2$CO and CH$_3$OH. It is believed that both species would form in the postshock gas after CO dissociates. For CH$_3$OH, CH$_4$+OH or CH$_3$+ H$_2$O could form CH$_3$OH in the postshock gas (Latter & Charnley 1996; Hartquist et al. 1995). H$_2$CO would form in a similar manner, with the reaction of O+CH$_3$ and then the release of a H atom (Cernicharo 2004). Another possible formation mechanism is H addition after the dissociation of CO in the postshock gas.

Grain surface reactions are also proposed to account for the abundance of oxygen-bearing molecules. For example, Watanabe et al. (2004 and references therein) have shown that H$_2$CO and CH$_3$OH can form from both CO and CO-H$_2$O ice sprayed with cold H. From this experiment they concluded that for an ISM environment with 1 H atom cm^{-3} and a temperature of 10 K, a timescale of 10^6 yr would be necessary to match observed CO/CH$_3$OH and H$_2$CO/CH$_3$OH ratios in molecular clouds. Subsequent H addition has also been theorized to produce complex oxygen-bearing organic molecules, including propenal (CH$_2$CHCHO) and propanal (CH$_3$CH$_2$CHO) (Hollis et al. 2004). To date, however, CH$_3$OH has not been detected toward

CRL 618, and the timescale of the PPN phase is only about 10 thousand years. It is apparent that this formation mechanism would be too slow to produce detectable amounts of CH_3OH in CRL 618.

Finally, there are also gas-phase reaction schemes that attempt to predict the abundance of oxygen-bearing organic molecules. To investigate whether gas-phase reactions may be responsible for the formation of oxygen-bearing organic molecules in the CSE of CRL 618, we used the gas-phase reactions of the UMIST database (Le Teuff et al. 2000) and compared the predicted fractional abundance to the upper limits measured from our survey. The limitation that we found on this procedure is the limited number of reactions to form the larger oxygen-bearing organic molecules. However, we can discuss two molecular formation models and how they compare to our measured upper limits. Furthermore, as a constraint on our analysis, we included only formation models that contained molecules already detected toward CRL 618 or molecules that are structurally similar to other species but have not yet been detected.

We adopt a measured UV flux of $\sim 3 \times 10^6$ photons s^{-1}, a n_{H_2} abundance of 10^7 cm^{-3}, and a temperature of 100 K (Herpin & Cernicharo 2000). The proposed gas-phase reaction formation of HCOOH is $HCO^+ + H_2O \rightarrow HCOOH_2^+$ and the destruction mechanism is $HCOOH + h\nu \rightarrow HCO + OH$. HCO^+ and H_2O have been detected in the CSE of CRL 618, and their fractional abundances have also been measured. The calculated fractional abundance of HCOOH based on the formation model is $\sim 5 \times 10^{-11}$. The calculated upper limit based on our observations is $X_{HCOOH} \sim 2 \times 10^{-9}$. Thus, the combination of a lower abundance of H_2O and HCO^+ and a higher UV ionization rate suggests that doubly oxygenated molecules have abundances that are still too low to detect. No other oxygen-bearing organic molecule that we searched for had any formation mechanism based on species already found in the CSE of CRL 618 or formation models listed in the UMIST database.

However, the situation is less clear for the singly oxygenated species such as CH_3CHO. The proposed gas-phase reaction formation of CH_3CHO is $O + C_2H_5 \rightarrow CH_3CHO + H$, and the destruction mechanism is $CH_3CHO + h\nu \rightarrow CO + CH_4$. C_2H_5 has not yet been detected in the CSE of CRL 618; however, C_2H_4 has been detected, and the fractional abundance has been measured as $\sim 10^{-4}$. The calculated fractional abundance of CH_3CHO based on the formation model is $\sim 5 \times 10^{-6}$. The calculated upper limit based on our observations is below this value, $X_{CH_3CHO} \sim 10^{-6}$. The implication for the formation and detection of CH_3CHO is that if the abundance of C_2H_5 is similar to that of C_2H_4, gas-phase reactions like those listed above are not important to the formation of this molecule.

One obvious difference between PPNe and molecular cores that may account for the difference in grain surface reactions is their different grain properties. In the cold-collapse phase of molecular cores, molecules are depleted onto ices, where hydrogenation then slowly changes the chemical composition of the mantles. The mantles are then evaporated during the hot-core phase, and the subsequent release of these mantle species into the gas phase can then drive the complex chemistry observed in hot molecular cores. The envelopes of AGB stars and PPNe, on the other hand, are the actual sites of the formation of carbon dust via the formation of polycyclic aromatic hydrocarbons (PAHs). Hence, grain properties are very different from star-forming cores, and the cold-collapse phase is completely lacking. Therefore, if grain chemistry and the subsequent processing of the grain mantle products in a hot-gas phase constitute the main route to produce large organic biomolecules in a large abundance, they cannot be expected to exist in PPNe. For further reviews of the chemistry leading to organic molecules, see Tielens & Charnley (1997) and Ehrenfreund & Charnley (2000). Indeed, while a complex chemistry is taking place toward PPNe, including CRL 618, it appears that the physical conditions and chemistry may not be efficient enough for large organic biomolecules to be produced and detected.

5. SUMMARY

We have presented the results of our survey toward the proto–planetary nebula CRL 618 for several large, highly saturated organic molecules of biological importance including acetaldehyde (CH_3CHO), acetic acid (CH_3COOH), dimethyl ether (CH_3OCH_3), ethanol (CH_3CH_2OH), formic acid (HCOOH), and methyl formate ($HCOOCH_3$); large carbon chain molecules including methyl cyanide (CH_3CN), methylcyanoacetylene (CH_3C_3N), cyanoacetylene (HC_3N), cyanodiacetylene (HC_5N), and C_6H; and, finally, smaller molecules including ^{34}SO, SO_2, $OC^{34}S$, and MgNC. No biologically important organic molecules were detected. However, based on the 1 σ rms noise level in the spectral windows containing our large molecular species, we were able to place upper limits on the column density and fractional abundances relative to H_2 (Table 4). We made the first interferometric detection of CH_3CN toward CRL 618. Using a rotational temperature diagram of the $J = 6-5$ rotational transitions, we found a temperature of 88 (44) K, and from the temperature and distribution of CH_3CN toward CRL 618, we find that CH_3CN is formed in the outer envelope surrounding the UC H II region. We also made the first interferometric detection of vibrationally excited HC_5N toward this source, as well as detections of transitions of the $\nu_7 = 3$ and 4 states of HC_3N. The P Cygni line profile and corresponding channel maps of vibrationally excited HC_5N supports its distribution in the extended CSE expanding away from the central star. The detection of vibrationally excited HC_3N confirmed the temperature structure and column density of HC_3N in the extended envelope found by Wyrowski et al. (2003). Finally, our observations clearly indicate that CRL 618 is a good source of large carbon chain species but a very poor source for detecting or producing organic species of biological importance.

REFERENCES

Bauder, A., Lovas, F. J., & Johnson, D. R. 1976, J. Phys. Chem. Ref. Data, 5, 53
Boucher, D., Burie, J., Bauer, A., Dubrulle, A., & Demaison, J. 1980, J. Phys. Chem. Ref. Data, 9, 659
Bujarrabal, V., Bachiller, R., Alcolea, J., & Martin-Pintado, J. 1988, A&A, 206, L17
Cernicharo, J. 2004, ApJ, 608, L41
Cernicharo, J., Guelin, M., Martin-Pintado, J., Penalver, J., & Mauersberger, R. 1989, A&A, 222, L1
Cernicharo, J., Heras, A. M., Pardo, J. R., Tielens, A. G. G. M., Guelin, M., Dartois, E., Neri, R., & Waters, L. B. F. M. 2001a, ApJ, 546, L127
Cernicharo, J., Heras, A. M., Tielens, A. G. G. M., Pardo, J. R., Herpin, F., Guelin, M., & Waters, L. B. F. M. 2001b, ApJ, 546, L123
Cummins, S. E., Green, S., Thaddeus, P., & Linke, R. A. 1983, ApJ, 266, 331
Ehrenfreund, P., Bernstein, M. P., Dworkin, J. P., Sandford, S. A., & Allamandola, L. J. 2001, ApJ, 550, L95

Ehrenfreund, P., & Charnley, S. B. 2000, ARA&A, 38, 427

Friedel, D. N., Snyder, L. E., Turner, B. E., & Remijan, A. 2004, ApJ, 600, 234

Fukasaku, S., Hirahara, Y., Masuda, A., Kawaguchi, K., Ishikawa, S., Kaifu, N., & Irvine, W. M. 1994, ApJ, 437, 410

Goldsmith, P. F., & Langer, W. D. 1999, ApJ, 517, 209

Groner, P., Albert, S., Herbst, E., & de Lucia, F. C. 1998, ApJ, 500, 1059

Guelin, M., & Cernicharo, J. 1991, A&A, 244, 21L

Hartquist, T. W., Menten, K. M., Lepp, S., & Dalgarno, A. 1995, MNRAS, 272, 184

Hasegawa, T. I., Herbst, E., & Leung, C. M. 1992, ApJS, 82, 167

Herpin, F., & Cernicharo, J. 2000, ApJ, 530, L129

Herpin, F., Goicoechea, J. R., Pardo, J. R., & Cernicharo, J. 2002, ApJ, 577, 961

Highberger, J. L., & Ziurys, L. M. 2003, ApJ, 597, 1065

Hollenbach, D., & Salpeter, E. E. 1971, ApJ, 163, 155

Hollis, J. M., Jewell, P. R., Lovas, F. J., Remijan, A., & Møllendal, H. 2004, ApJ, 610, L21

Ilyushin, V. V., et al. 2001, J. Mol. Spectrosc., 205, 286

Jennings, D. E., & Fox, K. 1982, ApJ, 254, 111

Latter, W. B., & Charnley, S. B. 1996, ApJ, 463, L37

Le Teuff, Y. H., Millar, T. J., & Markwick, A. J. 2000, A&AS, 146, 157

Liu, S.-Y., Girart, J. M., Remijan, A., & Snyder, L. E. 2002, ApJ, 576, 255

Lovas, F. J. 1982, J. Phys. Chem. Ref. Data, 11, 251

Maki, A. G. 1974, J. Phys. Chem. Ref. Data, 3, 221

Mehringer, D. M., & Snyder, L. E. 1996, ApJ, 471, 897

Müller, H. S. P., Thorwirth, S., Roth, D. A., & Winnewisser, G. 2001, A&A, 370, L49

Oesterling, L. C., Albert, S., de Lucia, F. C., Sastry, K. V. L. N., & Herbst, E. 1999, ApJ, 521, 255

Pardo, J. R., Cernicharo, J., Goicoechea, J. R., & Phillips, T. G. 2004, ApJ, 615, 495

Pickett, H. M., Poynter, R. L., Cohen, E. A., Delitsky, M. L., Pearson, J. C., & Muller, H. S. P. 1998, J. Quant. Spectrosc. Radiat. Transfer, 60, 883

Remijan, A., Shiao, Y.-S., Friedel, D. N., Meier, D. S., & Snyder, L. E. 2004a, ApJ, 617, 384

Remijan, A., Snyder, L. E., Friedel, D. N., Liu, S.-Y., & Shah, R. Y. 2003, ApJ, 590, 314

Remijan, A., Snyder, L. E., Liu, S.-Y., Mehringer, D. M., & Kuan, Y.-J. 2002, ApJ, 576, 264

Remijan, A., Sutton, E. C., Snyder, L. E., Friedel, D. N., Liu, S.-Y., & Pei, C. C. 2004b, ApJ, 606, 917

Sanchez Contreras, C., & Sahai, R. 2004, ApJ, 602, 960

Sault, R. J., Teuben, P. J., & Wright, M. C. H. 1995, in ASP Conf. Ser. 77, Astronomical Data Analysis Software and Systems IV, ed. R. A. Shaw, H. E. Payne, & J. J. E. Hayes (San Francisco: ASP), 433

Snyder, L. E., Lovas, F. J., Mehringer, D. M., Miao, N. Y., Kuan, Y.-J., Hollis, J. M., & Jewell, P. R. 2002, ApJ, 578, 245

Solomon, P. M., Jefferts, K. B., Penzias, A. A., & Wilson, R. W. 1971, ApJ, 168, L107

Sutton, E. C., Blake, G. A., Genzel, R., Masson, C. R., & Phillips, T. G. 1986, ApJ, 311, 921

Thorwirth, S. 2001, Ph.D. thesis, Univ. Köln

Thorwirth, S., Wyrowski, F., Schilke, P., Menten, K. M., Brünken, S., Müller, H. S. P., & Winnewisser, G. 2003, ApJ, 586, 338

Tielens, A. G. G. M., & Charnley, S. B. 1997, Origins Life Evolution Biosphere, 27, 23

Tielens, A. G. G. M., & Hagen, W. 1982, A&A, 114, 245

Tiemann, E. J. 1974, J. Phys. Chem. Ref. Data, 3, 259

Trammell, S. R. 2000, in ASP Conf. Ser. 199, Asymmetrical Planetary Nebulae II: From Origins to Microstructures, ed. J. Kastner, N. Soker, & S. Rappaport (San Francisco: ASP), 147

Ueta, T., Fong, D., & Meixner, M. 2001, ApJ, 557, L117

Watanabe, N., Nagaoka, A., Shiraki, T., & Kouchi, A. 2004, ApJ, 616, 638

Willemot, E., Dangoisse, D., Monnanteuil, N., & Bellet, J. 1980, J. Phys. Chem. Ref. Data, 9, 59

Winnewisser, G., & Walmsley, C. M. 1978, A&A, 70, 37L

Woods, P. M., Millar, T. J., Herbst, E., & Zijlstra, A. A. 2003, A&A, 402, 189

Wyrowski, F., Schilke, P., Thorwirth, S., Menten, K. M., & Winnewisser, G. 2003, ApJ, 586, 344

Wyrowski, F., Schilke, P., & Walmsley, C. M. 1999, A&A, 341, 882

Yamada, K. M. T., & Creswell, R. A. 1986, J. Mol. Spectrosc. 116, 384

Yamada, K. M. T., Degli Esposti, C., Botschwina, P., Förster, P., Bizzocchi, L., Thorwirth, S., & Winnewisser, G. 2004, A&A, 425, 767